




# Structural studies and physical properties of Gd<sub>2</sub>O<sub>3</sub>-doped borate glass

M. A. Madshal<sup>1,2,\*</sup> , G. El-Damrawi<sup>1</sup>, A. M. Abdelghany<sup>3,4</sup>, and M. I. Abdelghany<sup>1</sup>

<sup>1</sup>Glass Research Group, Physics Department, Faculty of Science, Mansoura University, Mansoura 35516, Egypt

<sup>2</sup>Physics Department, Faculty of Science, Sana'a University, Sana'a, Yemen

<sup>3</sup>Physics Division, Spectroscopy Department, National Research Center, 33 Elbehouth St., Dokki, Giza 12311, Egypt

<sup>4</sup>Basic Science Department, Horus University, Costal Road, New Damietta, Egypt

Received: 16 March 2021

Accepted: 18 April 2021

Published online:  
6 May 2021

© The Author(s), under exclusive licence to Springer Science+Business Media, LLC, part of Springer Nature 2021

## ABSTRACT

Gd<sub>2</sub>O<sub>3</sub>-doped glasses in the B<sub>2</sub>O<sub>3</sub>–CaO–Na<sub>2</sub>O–SrO–P<sub>2</sub>O<sub>5</sub> system were synthesized via melt annealing route and characterized through physical properties. With the replacement of CaO by Gd<sub>2</sub>O<sub>3</sub>, the measured values of the density ( $d_s$ ), Gd<sup>3+</sup> ions concentration (N), packing density ( $P_d$ ), oxygen packing density (OPD), Vickers's hardness ( $H_V$ ), and field strength (F) of the synthesized samples increased, whereas the molar volume ( $V_m$ ), free volume ( $V_f$ ), polaron radius ( $r_p$ ), average boron–boron distance ( $d_{B-B}$ ), and inter-nuclear distance ( $r_i$ ) decreased. The glassy nature of the synthesized samples is confirmed by the X-ray diffraction patterns. The change in the coordination number of boron and the different B–O vibrational bands with the incorporation of gadolinium ions in the investigated glass samples were examined by Raman and FTIR spectroscopy, which supported the presence of BO<sub>3</sub>, BO<sub>4</sub>, and GdO<sub>4</sub> groups.

## 1 Introduction

Borate glasses containing rare-earth oxide are among the most important materials which have been invented since ancient time. They were considered as useful materials in different field applications [1–3]. Due to the potential practical applications in advanced laser materials [4], optical, memory devices [5], and biomaterials glass fields [6], the study of the borate glass is of great interest for basic research. In recent years, borate-based glasses are very important because of their interesting chemical and physical

properties such as their significantly lower melting temperature, low viscosity, good mechanical stability, low chemical durability, attainability at low cost, and high visible light transparency [7–9]. It is known that in silicate glass, silicon is present in SiO<sub>4</sub> [10]. In contrast to silicate glass, vitreous borate glasses contain a mixture of triangles units BO<sub>3</sub> and tetrahedral units BO<sub>4</sub> depending on the composition of the glass [11]. Incorporation of the network-modifying cations such as (CaO, SrO, and Na<sub>2</sub>O) into the borate matrix glass is suggested to modify the network structure and change the environment of the glass network

Address correspondence to E-mail: mahdimadshal01010@gmail.com

[3, 6, 12, 13]. These modifiers will either be used to break one of the three bonds between boroxol rings to convert boron from a three-coordinated ( $\text{BO}_3$ ) unit to a four-coordinated ( $\text{BO}_4$ ) unit or to create non-bridging NBOs depending on the concentrations of the  $\text{B}_2\text{O}_3$  as a former and these modifiers [14]. Depending on the type and amount of the modifier oxide, the maxima of the fraction of boron in tetrahedral coordination ( $\text{N}_4$ ) occurs around 35–45 mol% [15]. It has been reported that the transformation between  $\text{BO}_3$  and  $\text{BO}_4$  boron groups as a function of the composition has a major influence on properties of glass such as its density, hardness, and molar volume ( $V_m$ ) [16]. Strontium is an alkaline earth metal which falls after calcium in the periodic table and shares many similar properties [17]. The presence of SrO as well as CaO in the glass compositions causes increase in the density, structural rigidity [18], and enhances the bioactive properties of borate glasses [19]. Nowadays, transition metal, lanthanide and, rare-earth oxide doped glass and glass-ceramic are of increasing interest in various types of applications such as optical [20], electrical [21], and biomedical application [22]. The rare-earth oxide is used as a glass dopant to probe the glass environment's structure due to its sharp energy levels and the modifications of the energy level of the modifier ions structure by the glassy environment [23]. In general, lanthanides are stable as trivalent ions in most glass synthesized using the conventional melt technique. As a classic lanthanide element, studies on  $\text{Gd}_2\text{O}_3$  containing borate glasses are limited. The structural roles of the alkali and alkaline earth oxides are well known in borate glass, but the role of  $\text{Gd}_2\text{O}_3$  in such is not well known especially in bioborate glass systems. Therefore, our study is to evaluate the structural variation induced by  $\text{Gd}_2\text{O}_3$  and identify its influence on the physical properties of borate-based glass.

## 2 Experimental work and techniques

### 2.1 Sample preparation

Glass samples were synthesized by using high-purity analytical grade chemical as reserved. Gadolinium oxide ( $\text{Gd}_2\text{O}_3$ , Sigma-Aldrich 99.9%) was introduced as such,  $\text{B}_2\text{O}_3$  was introduced as  $\text{H}_3\text{BO}_3$  (Sigma-Aldrich, 99.5%), Ammonium dihydrogen

orthophosphate ( $\text{NH}_4\text{H}_2\text{PO}_4$ , Sigma-Aldrich 98%) was used as the source for  $\text{P}_2\text{O}_5$ , SrO was introduced as  $\text{SrCO}_3$  (98.5%, Sigma-Aldrich, Germany), CaO and  $\text{Na}_2\text{O}$  supplied by Aldrich company were also introduced as  $\text{CaCO}_3$  (99%) and  $\text{Na}_2\text{CO}_3$  (99%), respectively, which were used as starting materials to synthesize glass samples with composition  $42.7\text{B}_2\text{O}_3 - (23.5 - x)\text{CaO} - 26\text{Na}_2\text{O} - 5\text{SrO} - 2.8\text{P}_2\text{O}_5 - x\text{Gd}_2\text{O}_3$ , where  $0 < x < 0.5$  mol% (Table 1).

The electronic beam balance technique with an accuracy of 0.0001 g was used to weigh the chemical powders, and they were mixed with appropriate amounts of raw materials. The batches were put into the porcelain crucibles and then melted in the programmable electrical furnace at 1070–1150 °C for 60 min. After occasionally stirring the molten liquid for many times to ensure homogenizing the melt and to obtain bubble-free samples, they were cast into preheated (at 300 °C) stainless steel plates of the required dimensions and subsequently annealed for 1 h and then cooled slowly to room temperature to remove the thermal and internal stress from the samples. The glass samples in this research are colorless.

## 2.2 Spectroscopic investigations

### 2.2.1 X-ray spectroscopy

X-ray diffraction diffractogram of the synthesized samples was obtained by a Bruker Axs-D8 technique using a source  $\text{CuK}\alpha$  radiation ( $\lambda_{\text{CuK}\alpha} = 0.1540600$  nm). X-ray diffractometer operates at 40 kV as accelerating voltage and 30 mA current in the intervals of  $0.02^\circ$ , over a 2 theta ranging from  $4^\circ$  to  $70^\circ$  using a time of 0.4 s. Data were fitted with an Advantech super speed position-sensitive detector.

**Table 1** Samples nomination and composition

Sample	$\text{B}_2\text{O}_3$ Mol%	CaO	SrO	$\text{Na}_2\text{O}$	$\text{P}_2\text{O}_5$	$\text{Gd}_2\text{O}_3$
$G_0$	42.7	23.5	5	26	2.8	0.0
$G_1$	42.7	23.4	5	26	2.8	0.1
$G_2$	42.7	23.3	5	26	2.8	0.2
$G_3$	42.7	23.2	5	26	2.8	0.3
$G_4$	42.7	23.1	5	26	2.8	0.4
$G_5$	42.7	23.0	5	26	2.8	0.5

### 2.2.2 FTIR spectroscopy

FTIR spectra were obtained using FTIR spectroscopy (Mattson 5000, USA) for all the observed glasses in the wavenumber range 400–4000  $\text{cm}^{-1}$  at 2.0  $\text{cm}^{-1}$  resolution to perform the function group of these samples. Phosphate, borate, and the hydroxyl groups were characterized. To obtain good quality spectra, the glassy specimens were grinded to powder and dispersed in KBr in the ratio 1:100. The mixture was subjected to a constant pressure of 5 ton  $\text{cm}^{-2}$ . Clear transparent discs were obtained and measured immediately after preparation. The dark current noises and the background of the obtained IR spectra were corrected using two-point baseline correction before fitting.

### 2.2.3 Raman mapping spectroscopy

Raman spectra of the undoped glass and glass containing  $\text{Gd}_2\text{O}_3$  were recorded using a Renishaw in Via Raman microscope with a laser line at 632.8 nm wavelength to excite the specimen. It is operating at 500 mW and for each scan eight acquisitions were taken.

### 2.2.4 Physical properties

**2.2.4.1 Density and molar volume measurements** Archimedes' principle was used to measure the glass density ( $d_s$ ) at room temperature (30 °C) for all prepared bulk samples using Xylene as an immersion liquid (density = 0.865  $\text{g cm}^{-3}$ ). A digital balance (Mettler-Toledo, with error  $\pm 0.0001$  g) was used to weigh the bulk solid in air ( $W_{\text{SA}}$ ) as well as in the solvent ( $W_{\text{SL}}$ ), and the  $d_s$  is calculated according to the following equation [24]:

$$d_s = \left[ \frac{W_{\text{SA}}}{W_{\text{SA}} - W_{\text{SL}}} \right] \times d_L, \quad (1)$$

where  $d_s$  is the density of the sample,  $W_{\text{SA}}$  and  $W_{\text{SL}}$  are the weights of the sample in the air and liquid, respectively, and  $d_L$  is the density of the Xylene. The density measurements were carried out on three samples of each glass, and the average value was calculated. Density values are precise to  $\pm 0.002$   $\text{g cm}^{-3}$ .

The  $V_m$  is defined as the volume of the substance containing one mol%.  $V_m$  of the prepared glass

samples were calculated from the obtained density data using the formula [24]:

$$V_m = \sum \frac{n_i M_i}{d_s}, \quad (2)$$

where  $M_i$  is the molecular mass for a component  $i$ ,  $n_i$  is the molar ratio, and  $d_s$  is the density of the sample.

**2.2.4.2 Free volume ( $V_f$ ) and packing density ( $P_d$ )** The  $V_f$  was defined as the unoccupied space which exists between molecules, and it is used to explain the mobility of the molecular within the network. The  $V_f$  is given in the equation:

$$V_f = V_m - \sum x_i V_i, \quad (3)$$

where  $x_i$  is the molar ratio of the samples and  $V_i$  is the  $V_m$  of each component.

$P_d$  was defined as the ratio between the minimum fraction of volume occupied by the ions and the corresponding effective volume of glass [25].  $P_d$  was obtained using the next formula [25]:

$$P_d = \sum \frac{x_i V_i}{V_m}. \quad (4)$$

OPD is considered as a measure of packing oxide network tightening of the prepared glass samples and can be evaluated by applying the relation [26]:

$$\text{OPD} = n \left( \frac{d_s}{M} \right) \times 1000, \quad (5)$$

where  $M$  is the average molecular weight and  $n$  is the number of oxygen atoms per formula unit.

The effect of dopant concentration in the glass matrix can be identified by the average boron–boron separation according to the following relation [27]:

$$\langle d_{\text{B-B}} \rangle = \left[ \frac{V_m^b}{N_A} \right]^{\frac{1}{3}}, \quad (6)$$

where  $V_m^b$  is the molar volume of boron atoms and is given by

$$V_m^b = \frac{V_m}{2(1 - X_B)}, \quad (7)$$

where  $X_B$  is the mole fraction of  $\text{B}_2\text{O}_3$  content.

**2.2.4.3 Ion concentration (N)** The  $\text{Gd}^{3+}$  ions concentration (N) is calculated using the equation [28]

$$N = \frac{\text{Mol\% of dopant} \times \text{Density of sample } (d_s) \times \text{Avogadro's No.}}{\text{Glass average molecular mass}} \quad (8)$$

A polaron was defined as a quasi-particle which is used to describe the interaction between the electrons and ions and also used to understand the interaction between the electrons and atoms in the solid materials. The polaron radius ( $r_p$ ) in (Å) can be evaluated depending on the value obtained of N, using the following equation [29]:

$$r_p(\text{Å}) = \frac{1}{2} \left[ \frac{\pi}{6N} \right]^{\frac{1}{3}} \quad (9)$$

The inter-nuclear distance ( $r_i$ ) was calculated according to the next expression [30]:

$$r_i(\text{Å}) = \left( \frac{1}{N} \right)^{\frac{1}{3}} \quad (10)$$

The field strength (F) can be evaluated using the equations [30]:

$$F = \left( \frac{Z}{r_p^2} \right), \quad (11)$$

where Z the molar mass of the rare earth (gadolinium oxide).

**2.2.4.4 Microhardness measurements ( $H_V$ )** The hardness of the specimens was determined using a digital Vickers microscope model (FM-7, Future-Tech Corporation, Kawasaki-Japan). The Vickers's hardness ( $H_V$ ) test was performed under 50 g load and 15 s of dwell time. The sample surface was polished, and twelve indentations were made on the surface of each specimen at room temperature and the average value of the diagonal was used to calculate  $H_V$  from the following equation [31]:

$$H_V = 1.854 F/d^2(2.3), \quad (12)$$

where F is the applied indentation load in kgf, and d is the arithmetic mean of the two measured indentation diagonals  $d_1$  and  $d_2$  in mm. The applied indentation load was calculated using the following formula:

$$F = Kd^n \quad (13)$$

$$\log F = \log K + n \log d, \quad (14)$$

where n is Meyer's index number, K is the substance constant, n value was obtained from the plot of logF

versus logd since the slope of the line yields represent the value of n, which indicates whether the substance is hard or soft.

### 3 Result and dissection

#### 3.1 X-ray analysis

The nature of the glassy materials can be understood using X-ray powder diffraction, but this approach is particularly useful for the analysis of the glassy materials network. Figure 1 shows the X-ray diffraction spectra of the  $B_2O_3$ -CaO- $Na_2O$ -SrO- $P_2O_5$  glass system containing different concentrations of  $Gd_2O_3$ . Broadband appears in the wide range ( $2\theta = 25^\circ$ - $35^\circ$ ) and showed no identifiable diffraction peaks indicating that  $Gd_2O_3$  containing glass has amorphous nature.

#### 3.2 Vibrational spectroscopy

FTIR and Raman spectroscopies are powerful tools for structural analysis and are used as complementary techniques. They used with advantage to understand the structure and environment of the matrix, although they differ slightly from the working principle. The Raman spectra depend on the change of the polarizability. On the other hand, the bands arise from the polarizability change due to the scattering of light by the vibrating molecules, whereas the IR bands arise from the change in the dipole moments as a result of the absorption of light by molecules vibrations. A view of transitions are

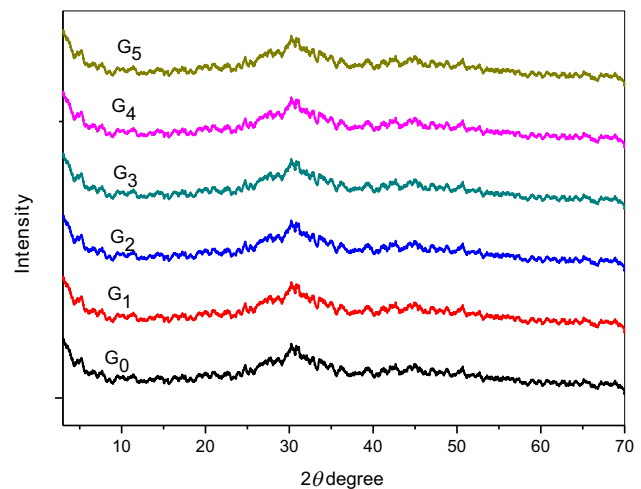


Fig. 1 X-ray spectra of all prepared glass samples

forbidden in IR spectroscopy, but they are allowed in Raman spectra [32]. These two techniques have been employed to know the functional groups present in the glass samples.

### 3.2.1 FTIR interpretation

Figure 2 demonstrates FTIR measurements in a region 400–4000  $\text{cm}^{-1}$  for the prepared glass samples. FTIR spectrum reported some bands at around 570, 708, 1022, 1220, and 1406  $\text{cm}^{-1}$ . The bands at about 1220–1406  $\text{cm}^{-1}$  are attributed to the vibration of the various borate groups (B–O bond stretch of the  $\text{BO}_3$  units) and related to B–O–B bending vibrations [33]. The band at about 1022  $\text{cm}^{-1}$  is attributed to the B–O bonding stretch of  $\text{BO}_4$  units [34]. The small band at 708  $\text{cm}^{-1}$  can be ascribed to the symmetric strength vibration of  $\text{BO}_3$  [34]. The peaks within the range 400–600  $\text{cm}^{-1}$  are assumed by some authors [34, 35] to represent vibrations of modifier cations ( $\text{Na}^+$ ,  $\text{Ca}^{2+}$ ) and bending mode of  $\text{PO}_4^{3-}$  in these glasses [35]. As we have observed, the band at around 570  $\text{cm}^{-1}$  described B–O–Gd, and Gd–O–Gd bending modes and  $\text{GdO}_4$ . The assignments for each FTIR bands are recorded in Table 2.

Peak fit program was used to de-convolute the FTIR spectra of all the prepared samples, and the deconvolution parameters are given in Table 4 in Appendix. The FTIR spectra were corrected from the dark current noises and background using two points of baseline correction before fitting previously discussed [36, 37]. Figure 3a, b displays the FTIR deconvolution, in Gaussian band, and the residual graph for  $42.7\text{B}_2\text{O}_3\text{--}23.4\text{CaO--}26\text{Na}_2\text{O--}5\text{SrO--}2.8\text{P}_2\text{O}_5\text{--}$

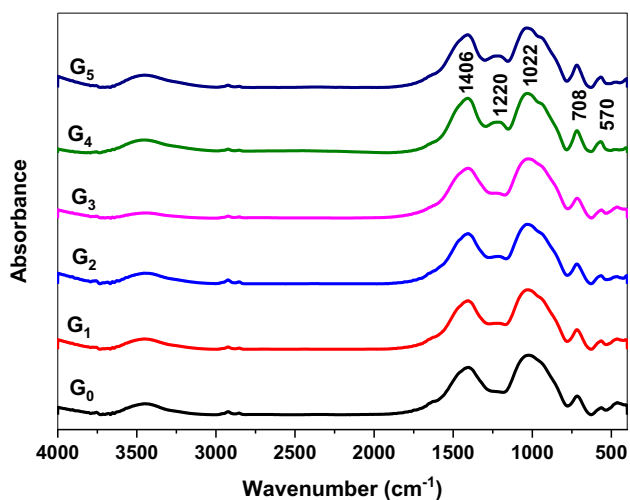


Fig. 2 FTIR spectra of all the prepared glass samples

$0.1\text{Gd}_2\text{O}_3$  sample, respectively, as an example. It was found that the difference between the experimental and simulated curves is less than 0.05% as can be seen in Fig. 3b. And then  $\text{BO}_3$  and  $\text{BO}_4$  peaks areas were integrated to calculate the  $N_4$  using the next formula:

$$N_4 = \frac{\text{BO}_4}{\text{BO}_3 + \text{BO}_4}. \quad (15)$$

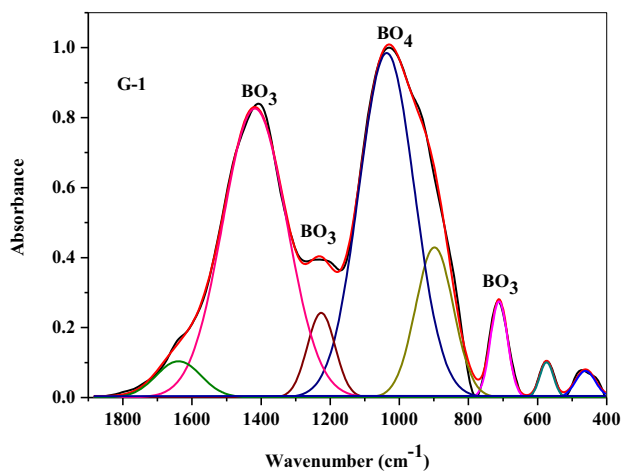
Figure 4 displays the  $N_4$  as a function of  $\text{Gd}_2\text{O}_3$  content to estimate the  $\text{Gd}_2\text{O}_3$  effect on the change of the relative population of tetrahedral units  $\text{BO}_4$  and triangle units  $\text{BO}_3$ . It is observed that  $N_4$  values varied between 0.47980 and 0.51502 according to the  $\text{Gd}_2\text{O}_3$  concentration. It would appear that the addition of  $\text{Gd}_2\text{O}_3$  tends to decrease  $\text{BO}_4$  units.

### 3.2.2 Raman spectroscopy analysis

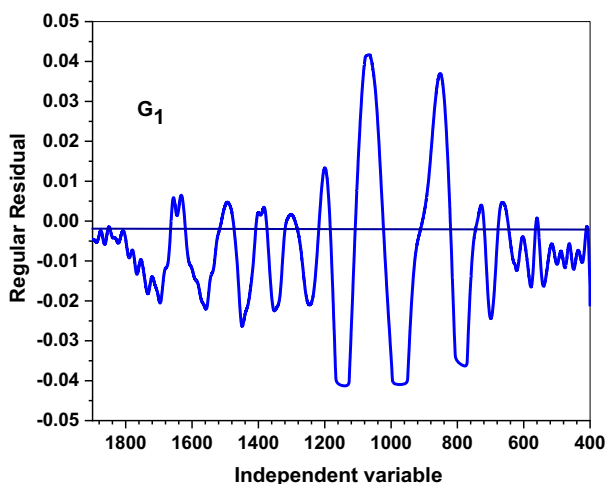
Normalized Raman spectra of the studied undoped glass and glasses containing different concentrations of  $\text{Gd}_2\text{O}_3$  are shown in Fig. 5. Raman spectra consist of three major regions to clarify the effects of  $\text{Gd}_2\text{O}_3$  in the glass network. The first is the low-wavenumber region extending from 400 to 600  $\text{cm}^{-1}$ . The second is a mid-wavenumber region extending from 600 to 1100  $\text{cm}^{-1}$ . Besides, the high wavenumber region falls between 1100 and 1600  $\text{cm}^{-1}$ . Previous studies indicate that the Raman spectrum of the vitreous  $\text{B}_2\text{O}_3$  is dominated by a strongly polarized intense band at 810  $\text{cm}^{-1}$ , which evidences that  $\text{B}_2\text{O}_3$  glass consists mainly of boroxol rings, the band at 810  $\text{cm}^{-1}$  being the characteristic feature [38–40]. But when the alkali and alkaline earth oxide were added, several changes occurred in the network of borate glass [38]. For example, the band at 810  $\text{cm}^{-1}$  disappears in almost all of alkali and alkali earth borate glass for > 20 mol% [38], such as in the present work. The Raman spectrum of the present work (Fig. 5) does not contain a band at around 810  $\text{cm}^{-1}$ , which indicates that most of the boroxol rings were converted to diborate (in which  $\text{BO}_3$  and  $\text{BO}_4$  are equal), triborate, and dipentaborate groups. The most notable is that, in the mid-frequency region (600–1100  $\text{cm}^{-1}$ ) of the measured spectra, the Raman bands displayed a strong peak due to B–O vibrations, since the glasses under investigation are low in  $\text{Gd}_2\text{O}_3$  and strong in  $\text{B}_2\text{O}_3$  concentrations. And the sharpening of this peak in the free and containing  $\text{Gd}_2\text{O}_3$  glass correlates usually to the asymmetric vibrations of pentaborate,

**Table 2** Peaks position and bands assignment of FTIR and Raman spectra for investigated samples

FTIR band		Raman band	
Band center (cm <sup>-1</sup> )	Assignment	Band center (cm <sup>-1</sup> )	Assignment
400–580	Vibrations of modifier cations (Na <sup>+</sup> , Ca <sup>2+</sup> ) and bending mode of PO <sub>4</sub> <sup>3-</sup>	400–600	Loose diborate & BO <sub>4</sub> groups due to the higher alkali oxide content [], and typically originates from B–O–B, Gd–O–Gd, and B–O–Gd stretching in units
708	Symmetric strength vibration of BO <sub>3</sub>	600–800	The six-membered rings with BO <sub>4</sub> <sup>-</sup> units
1022	B–O bonding stretch of BO <sub>4</sub> units	900–1100	of pentaborate, tetraborate and connected to the diborate groups
1220–1406	B–O bond stretch of the BO <sub>3</sub> units and B–O–B bending	1400–1550	the vibration of B–O <sup>-</sup> the BO <sub>3</sub> units



(a)



(b)

**Fig. 3** a De-convolution of the FTIR spectrum of one selected sample (G<sub>1</sub>), b residual of IR de-convolution of one selected sample (G<sub>1</sub>)

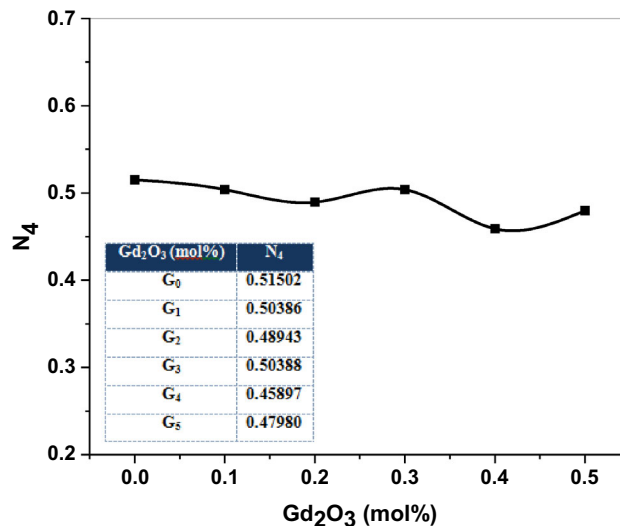


**Fig. 4** N<sub>4</sub> values versus Gd<sub>2</sub>O<sub>3</sub> mol%

tetraborate, and connected to the diborate groups (947 cm<sup>-1</sup>) [39, 40]. The band at about 761 cm<sup>-1</sup> is attributed to the six-membered rings with BO<sub>4</sub><sup>-</sup> units [36]. The low-frequency broadband centered at about 500 cm<sup>-1</sup> is assigned to the loose diborate & BO<sub>4</sub> groups due to the higher alkali oxide content [40] and typically arises from B–O–B bending modes, Gd–O–Gd and B–O–Gd stretching vibration in units of BO<sub>4</sub> and GdO<sub>4</sub>. The band in the range of 400–600 cm<sup>-1</sup> is attributed to the bridging anion mode of heavy metal oxide [41]. The formation of GdO<sub>4</sub> is depicted by the band at 500 cm<sup>-1</sup> due to the vibration of Gd<sub>4</sub>–O–Gd<sub>4</sub>.

With growing Gd<sub>2</sub>O<sub>3</sub> content, the relative area under the bands and the band's amplitude are increased due to the vibrations of GdO<sub>4</sub> tetrahedral

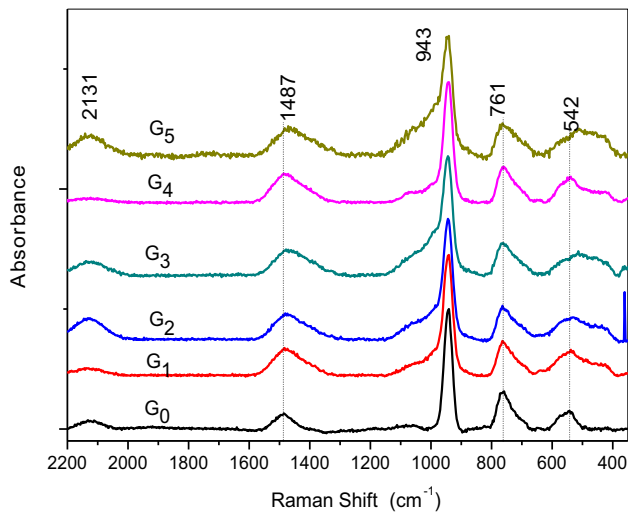


**Fig. 5** Normalized Raman spectra of all the prepared glass samples

units containing bridging oxygen (BO) and non-bridging oxygen (NBO). Finally, the Raman spectra include a medium band at about  $1487\text{ cm}^{-1}$  which appears at a higher frequency area and is assigned to the vibration of  $\text{B-O}^-$  the  $\text{BO}_3$  units, occurring in a large borate network. This band contains contributions from symmetrical triangle boron units [40]. From the above discussion, it is found that the Raman and FTIR results supported the presence of  $\text{BO}_3$ ,  $\text{BO}_4$ , and  $\text{GdO}_4$  groups. Peaks' position of the Raman spectra is recorded in Table 2.

### 3.3 Physical properties

#### 3.3.1 Density and molar volume

Density and  $V_m$  of undoped glass and glasses containing gadolinium oxide are given in Table 3 and Fig. 6. It is observed that the density of the investigated samples increases from  $2.64$  to  $2.78\text{ g cm}^{-3}$  due to the increase of  $\text{Gd}_2\text{O}_3$  mol% (from 0.0 to 0.5 mol%).

This increase can be explained based on the lower atomic weight of  $\text{CaO}$  (atomic mass,  $Z_{\text{CaO}} = 56.08\text{ g mol}^{-1}$ ) as compared to  $\text{Gd}_2\text{O}_3$  (atomic mass,  $Z_{\text{Gd}_2\text{O}_3} = 362.4982\text{ g mol}^{-1}$ ). Moreover, the density of  $\text{Gd}_2\text{O}_3$  ( $7.41\text{ g cm}^{-3}$ ) is higher than  $\text{CaO}$  ( $3.34\text{ g cm}^{-3}$ ), leading to an increase in the density of the prepared samples.

Figure 7 shows that  $P_d$  displays a slight increase with the addition of  $\text{Gd}_2\text{O}_3$  content due to the increase in the number of the oxygen atoms resulting from higher atomic weight of  $\text{Gd}_2\text{O}_3$  [42]. It is

observed also from Fig. 6 and Table 3 that the  $V_m$  of the investigated glass samples is found to decrease from  $25.77$  to  $25.07\text{ cm}^3\text{ mol}^{-1}$ . The ionic radius of  $\text{Gd}$  ( $0.938\text{ \AA}$ ) is smaller than that of  $\text{Ca}$  ( $1\text{ \AA}$ ), therefore the decrease of  $V_m$  can be explained based on the substitution  $\text{CaO}$  by  $\text{Gd}_2\text{O}_3$  causing shrinkage of the glass network. The increase in the density values will lead to a decrease in the  $V_m$  due to the inverse relationship between them [42, 43]. Hence, the compactness of the synthesized glass will increase [44]. Besides, the  $V_m$  is affected also by the decreasing  $V_f$ . The substitution of  $\text{CaO}$  with  $\text{Gd}_2\text{O}_3$  has an effective influence on the inter-atomic spacing between the atoms or in bond length. The variation in the  $V_m$  was affected by the rearrangement of lattice within the glass network, the number of bonds per unit volume [45], and the stretching force constant of the bonds inside the glassy [45].

#### 3.3.2 Ion concentration, polaron radius, and field strength

The calculated values of physical parameters such as  $\text{Gd}^{3+}$  ions concentration,  $r_p$ ,  $r_i$ ,  $F$ , and OPD of the prepared glass samples were recorded in Table 3 and illustrated as functions of gadolinium concentration in Fig. 8a, b. They reveal that values of both  $\text{Gd}$  ions concentration and  $F$  are increased linearly according to the increase of the  $\text{Gd}_2\text{O}_3$  content, while the values of both  $r_p$  and  $r_i$  are decreased, which is a logical result where the atomic radius of gadolinium ( $238\text{ pm}$ ) is larger than that of the calcium ( $231\text{ pm}$ ). The decreasing of the  $r_p$  and  $r_i$  and the increasing values of  $F$  indicator to the stronger bond between  $\text{Gd-O}$ , which in turn producing stronger field around  $\text{Gd}^{3+}$  ions. It can be also observed from Table 3, that the decreases of the average boron-boron distance,  $\langle d_{\text{B-B}} \rangle$ , (nm) with increasing  $\text{Gd}_2\text{O}_3$  content denotes the increase in compactness of the glass network and also supports the increments in the glass density as discussed above. Increasing ion concentrations lead to decreases in  $r_p$  and inter-nuclear distance. The average molar mass of the synthesized samples also increases with the increasing  $\text{Gd}_2\text{O}_3$  content. One of the important physical parameters is OPD, which provides an insight into the structure of the prepared glass samples. It is observed that the OPD values increase with increasing  $\text{Gd}_2\text{O}_3$  content, this result is in agreement with density and  $V_m$  results. As a result, the addition of the  $\text{Gd}_2\text{O}_3$  makes the glass network high and tightly packed.

**Table 3** Physical properties of 42.7 B<sub>2</sub>O<sub>3</sub> (23.5–*x*) CaO–26Na<sub>2</sub>O–5SrO–2.8P<sub>2</sub>O<sub>5</sub>–*x*(Gd<sub>2</sub>O<sub>3</sub>) glasses system

Parameters	Glass code					
	G <sub>0</sub>	G <sub>1</sub>	G <sub>2</sub>	G <sub>3</sub>	G <sub>4</sub>	G <sub>5</sub>
Density ( <i>d<sub>s</sub></i> ) g cm <sup>-3</sup> ± 0.0002	2.6458	2.7040	2.7264	2.7452	2.7606	2.7802
Molar volume ( <i>V<sub>m</sub></i> ) cm <sup>3</sup> mol <sup>-1</sup> ± 0.0001	25.7701	25.3312	25.2321	25.1711	25.1400	25.0724
Packing density ( <i>P<sub>d</sub></i> )	0.59226	0.60483	0.60646	0.60806	0.61013	0.61149
Free volume ( <i>V<sub>f</sub></i> )	10.51	10.05	9.93	9.86	9.81	9.74
Average mol.wt. ( <i>M<sub>Av</sub></i> ) (g)	68.183	68.494	68.790	69.099	69.403	69.701
Ion concentration ( <i>N</i> ) (× 10 <sup>20</sup> ions cm <sup>-3</sup> )	–	0.238	0.477	0.717	0.958	1.2006
Polaron radius ( <i>r<sub>p</sub></i> ) (Å)	–	14.014	11.109	9.697	8.806	8.1675
Inter-nuclear distance ( <i>r<sub>i</sub></i> ) (Å)	–	34.781	27.560	24.065	21.856	20.270
Molar volume of the boron atoms ( <i>V<sub>m</sub><sup>b</sup></i> )	22.487	22.103	22.016	21.963	21.937	21.876
Field strength ( <i>F</i> ) × 10 <sup>16</sup> (cm <sup>-2</sup> )	–	1.85	2.94	3.86	4.67	5.43
Average boron–boron distance ( <i>d<sub>B-B</sub></i> ) (nm)	33.43	33.23	33.19	33.16	33.15	33.12
Oxygen packing density (OPD) (g atm l <sup>-1</sup> )	76.290	77.694	78.082	78.347	78.520	78.819
Hardness ( <i>H<sub>V</sub></i> ) (Kg mm <sup>-2</sup> ) ± 0.02	270.24	301.45	322.52	350.34	365.37	373.22

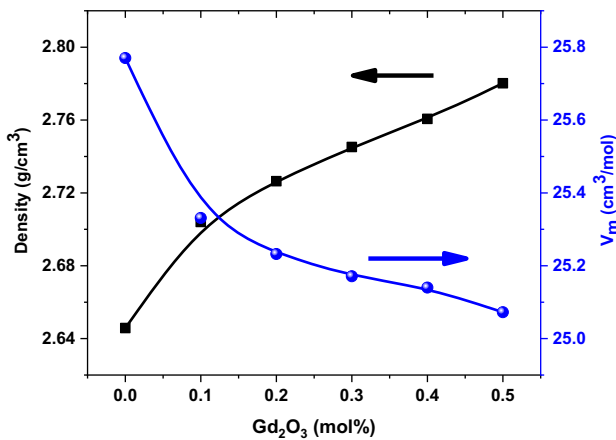


**Fig. 6** Density and *V<sub>m</sub>* of 42.7 B<sub>2</sub>O<sub>3</sub> (23.5–*x*) CaO–26Na<sub>2</sub>O–5SrO–2.8P<sub>2</sub>O<sub>5</sub>–*x*(Gd<sub>2</sub>O<sub>3</sub>) glass samples

3.3.3 Hardness of the prepared glass samples

Figure 9 represents the *H<sub>V</sub>* values as a function of the Gd<sub>2</sub>O<sub>3</sub> content. As noted below, the values of *H<sub>V</sub>* increase with increasing Gd<sub>2</sub>O<sub>3</sub> content, indicating the formation of a rigid structure which makes the glass harder. Cations that have smaller radii and high *F* are high and strongly attracted to the surrounding structural units of borate units. Therefore, it is worthy to note that the smaller radii and high *F* of Gd cations can affect the hardness number of borate glass. The increase in hardness and density is due to the higher molecular weight of Gd<sub>2</sub>O<sub>3</sub> (362.4982 g mol<sup>-1</sup>) compared with CaO (56.08 g mol<sup>-1</sup>), and coupled with high *F*. The presence of GdO<sub>4</sub>, BO<sub>3</sub>, & BO<sub>4</sub> groups in

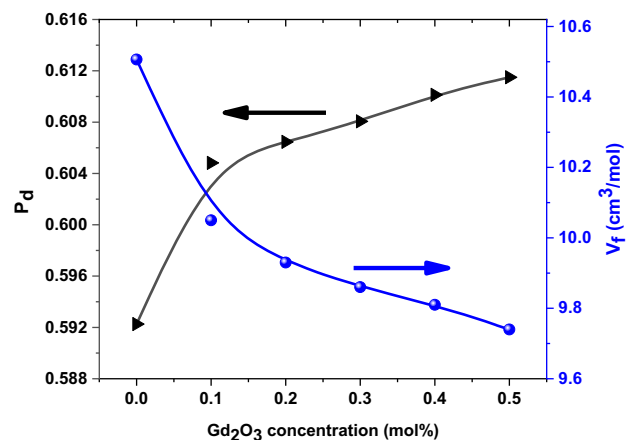


**Fig. 7** *P<sub>d</sub>* and *V<sub>f</sub>* of 42.7 B<sub>2</sub>O<sub>3</sub> (23.5–*x*)CaO–26Na<sub>2</sub>O–5SrO–2.8P<sub>2</sub>O<sub>5</sub>–*x*(Gd<sub>2</sub>O<sub>3</sub>) glass samples

the glass network causes an increase in the connectivity of the structure which leads to an increase in microhardness values. Therefore, the investigated samples become more compact (more tightly packed).

4 Conclusion

Borate glasses containing different concentrations of Gd<sub>2</sub>O<sub>3</sub> have been characterized using several techniques. XRD patterns of the investigated samples revealed amorphous nature. The changes in the FTIR and Raman spectra and physical properties due to the



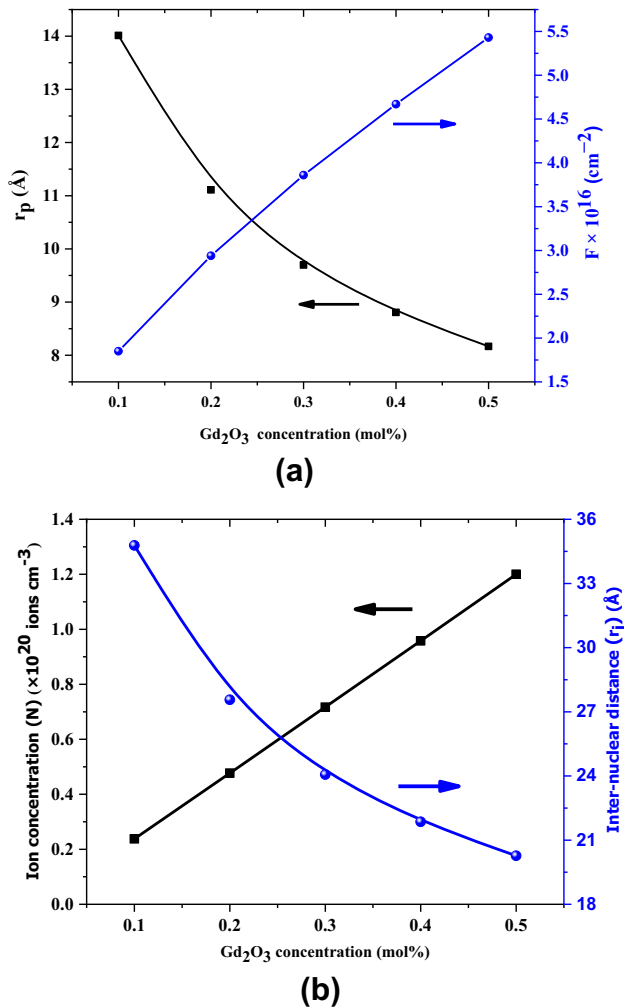


**Fig. 8** **a** Variation of both  $r_p$  and  $F$  as a function of Gd<sub>2</sub>O<sub>3</sub> content. **b** Variation of both  $N$  and  $r_i$  as a function of Gd<sub>2</sub>O<sub>3</sub> content

addition of Gd<sub>2</sub>O<sub>3</sub> contents result from the changes in bonding configuration, mainly Gd–O–B bonds and stretching vibrations of BO<sub>4</sub>, GdO<sub>4</sub>, and BO<sub>3</sub> units in the glass structure. The density values increase with increasing the heavier Gd<sub>2</sub>O<sub>3</sub> at the expense of lighter CaO content. The result of the Raman spectra supported the presence of GdO<sub>4</sub>, BO<sub>3</sub>, & BO<sub>4</sub>. The density,  $P_d$ , and microhardness of the prepared samples were found to be increased with Gd<sub>2</sub>O<sub>3</sub> content, while the  $V_m$  and  $V_f$  were found to decrease demonstrating an opposite trend. The presence of GdO<sub>4</sub>, BO<sub>3</sub>, & BO<sub>4</sub> groups in the glass network causes an increase in the connectivity of the structure which leads to an increase in microhardness values. Raman spectra revealed that the borate glasses network is affected by the addition Gd<sub>2</sub>O<sub>3</sub> content.

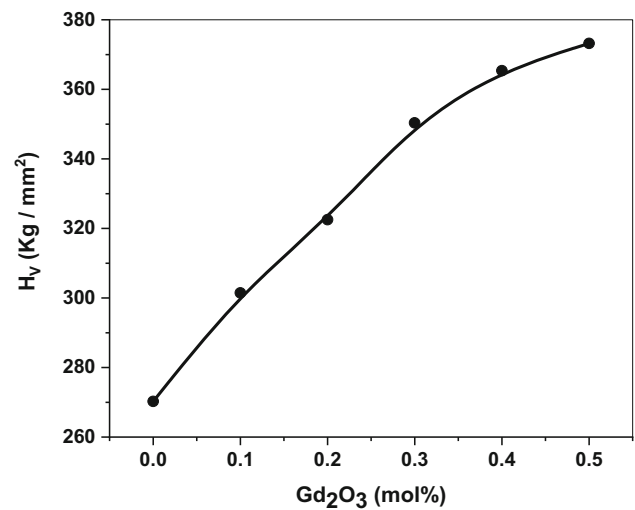


**Fig. 9** Dependence of microhardness ( $H_v$ ) on the concentration of Cr<sub>2</sub>O<sub>3</sub> (mol%)

### Author contributions

MAM: conceptualization, methodology, validation, investigation, writing—original draft, writing—review & editing, and visualization. GED: supervision, writing—review & editing. AMA: methodology and formal analysis. MIA: supervision.

### Funding

No funding. **Code availability**

Not applicable.

### Declarations

**Conflict of interest** The authors certify that they have no affiliations with or involvement in any organization or entity with any financial interest (such as honoraria; educational grants; participation in speakers' bureaus; membership, employment, consultancies, stock ownership, or other equity interest; and expert testimony or patent-licensing arrangements), or non-financial interest (such as personal or professional relationships, affiliations, knowledge, or beliefs) in the subject matter or materials discussed in this manuscript. The authors declare that they have no known competing financial interests or personal relationships that could have appeared to influence the work reported in this paper.

## Appendix

See Table 4.

**Table 4** De-convolution parameters of FTIR spectra of all prepared glass samples, where *B.C* is the band center ( $\text{cm}^{-1}$ ), *R.A.* is the relative area (%), and *A* is the area of the component bands

Gd <sub>2</sub> O <sub>3</sub> mol%	Structural units and band parameters								
0.0	<i>B.C</i>	576.65	708.42	906.57	1044.43	1231.48	1408.80	1594.4	
	<i>A</i>	6.9915	18.542	78.839	180.161	20.1737	169.949	35.228	
	<i>R.A</i>	0.0134	0.0356	0.1517	0.34680	0.03883	0.32714	0.0678	
	<i>group</i>		BO <sub>3</sub>	BO <sub>4</sub>	BO <sub>4</sub>	BO <sub>3</sub>	BO <sub>3</sub>	BO <sub>3</sub>	BO <sub>3</sub>
0.1	<i>B.C</i>	573.77	712.12	899.58	1036.48	1225.66	1418.82	1637.3	
	<i>A</i>	3.0223	14.687	56.723	192.026	25.6275	187.899	16.720	
	<i>R.A</i>	0.0060	0.0295	0.1141	0.38659	0.05159	0.37829	0.0336	
	<i>group</i>		BO <sub>3</sub>	BO <sub>4</sub>	BO <sub>4</sub>	BO <sub>3</sub>	BO <sub>3</sub>	H <sub>2</sub> O	
0.2	<i>B.C</i>	575.07	710.30	897.83	1036.06	1225.76	1413.62	1605.3	
	<i>A</i>	5.0688	17.336	58.787	190.289	30.7200	183.790	27.992	
	<i>R.A</i>	0.0098	0.0337	0.1143	0.37022	0.05976	0.35758	0.0544	
	<i>group</i>		BO <sub>3</sub>	BO <sub>4</sub>	BO <sub>4</sub>	BO <sub>3</sub>	BO <sub>3</sub>	H <sub>2</sub> O	
0.3	<i>B.C</i>	573.07	709.51	897.85	1036.09	1226.35	1414.34	1617.8	
	<i>A</i>	2.9894	15.360	62.568	194.713	17.1222	199.546	21.295	
	<i>R.A</i>	0.0058	0.0299	0.1218	0.37911	0.03333	0.38852	0.0414	
	<i>group</i>		BO <sub>3</sub>	BO <sub>4</sub>	BO <sub>4</sub>	BO <sub>3</sub>	BO <sub>3</sub>	H <sub>2</sub> O	
0.4	<i>B.C</i>	573.14	714.35	906.94	1039.99	1222.25	1417.46	1584.2	
	<i>A</i>	8.1532	20.228	77.957	161.737	53.1195	180.888	28.313	
	<i>R.A</i>	0.0153	0.0381	0.1469	0.30493	0.10015	0.34104	0.0533	
	<i>group</i>		BO <sub>3</sub>	BO <sub>4</sub>	BO <sub>4</sub>	BO <sub>3</sub>	BO <sub>3</sub>	BO <sub>3</sub>	
0.5	<i>B.C</i>	572.98	713.99	900.89	1036.68	1233.22	1406.44	1510.96	
	<i>A</i>	6.7925	19.569	66.770	174.659	63.7249	133.121	42.684	
	<i>R.A</i>	0.0126	0.0365	0.1247	0.32623	0.11902	0.24865	0.0797	
	<i>group</i>		BO <sub>3</sub>	BO <sub>4</sub>	BO <sub>4</sub>	BO <sub>3</sub>	BO <sub>3</sub>	BO <sub>3</sub>	

## References

- E.I. Kamitsos, G.D. Chryssikos, Borate glass structure by Raman and infrared spectroscopies. *J. Mol. Struct.* **247**, 1–16 (1991)
- M. Farouk, A. Samir, F. Metawe, M. Elokr, Optical absorption and structural studies of bismuth borate glasses containing Er<sup>3+</sup> ions. *J. Non. Cryst. Solids* **371**, 14–21 (2013)
- A.K. Yadav, P. Singh, A review of the structures of oxide glasses by Raman spectroscopy. *RSC Adv.* **5**(83), 67583–67609 (2015)
- V. Venkatramu, D. Navarro-Urrios, P. Babu, C.K. Jayasankar, V. Lavin, Fluorescence line narrowing spectral studies of Eu<sup>3+</sup>-doped lead borate glass. *J. Non. Cryst. Solids* **351**(10–11), 929–935 (2005)
- B. Sumalatha, I. Omkaram, T.R. Rao, C.L. Raju, The structural, optical and magnetic parameter of manganese doped strontium zinc borate glasses. *Phys. B Condens. Matter* **411**, 99–105 (2013)
- A.M. Abdelghany, M.A. Ouis, M.A. Azooz, H.A. ElBatal, G.T. El-Bassyouni, Role of SrO on the bioactivity behavior of some ternary borate glasses and their glass ceramic derivatives. *Spectrochim. Acta. Part A.* **152**, 126–133 (2016)
- M. Bengisu, Borate glasses for scientific and industrial applications: a review. *J. Mater. Sci.* **51**(5), 2199–2242 (2016)
- M. Mariyappan, K. Marimuthu, M.I. Sayyed, M.G. Dong, U. Kara, Effect Bi<sub>2</sub>O<sub>3</sub> on the physical, structural and radiation shielding properties of Er<sup>3+</sup> ions doped bismuth sodium fluoroborate glasses. *J. Non. Cryst. Solids* **499**, 75–85 (2018)
- S.B. Kolavekar, N.H. Ayachit, G. Jagannath, K. NagaKrishnakanth, S.V. Rao, Optical, structural and Near-IR NLO properties of gold nanoparticles doped sodium zinc borate glasses. *Opt. Mater. (Amst)* **83**, 34–42 (2018)
- K.H. Karlsson, K. Fröberg, Structural units in silicate glasses. *Chem. Geol.* **62**(1–2), 1–5 (1987)
- P. Naresh et al., Modifier role of ZnO on the structural and transport properties of lithium boro tellurite glasses. *J. Non. Cryst. Solids* **514**, 35–45 (2019)

12. G. Sangeetha, K.C. Sekhar, A. Hameed, G. Ramadevudu, M.N. Chary, M. Shareefuddin, Influence of CaO on the structure of zinc sodium tetra borate glasses containing  $\text{Cu}^{2+}$  ions. *J. Non. Cryst. Solids* **563**, 120784 (2021)
13. G. El-Damrawi, K. Abd-El-Nour, R.M. Ramadan, Structural and dielectric studies on  $\text{Na}_2\text{O}-\text{PbO}-\text{SiO}_2$  glasses. *SILICON* **11**(1), 495–500 (2019)
14. Y. Zhou, H. Li, K. Lin, W. Zhai, W. Gu, J. Chang, Effect of heat treatment on the properties of  $\text{SiO}_2-\text{CaO}-\text{MgO}-\text{P}_2\text{O}_5$  bioactive glasses. *J. Mater. Sci. Mater. Med.* **23**(9), 2101–2108 (2012)
15. W.C. Lepry, S.N. Nazhat, The anomaly in bioactive sol-gel borate glasses. *Mater. Adv.* **1**(5), 1371–1381 (2020)
16. M.S. Gaafar et al., Role of neodymium on some acoustic and physical properties of  $\text{Bi}_2\text{O}_3-\text{B}_2\text{O}_3-\text{SrO}$  glasses. *J. Mater. Res. Technol.* **9**(4), 7252–7261 (2020)
17. U. Patel et al., In vitro cellular testing of strontium/calcium substituted phosphate glass discs and microspheres shows potential for bone regeneration. *J. Tissue Eng. Regen. Med.* **13**(3), 396–405 (2019)
18. R. Divina, K.A. Naseer, K. Marimuthu, Y.S.M. Alajerami, M.S. Al-Buriahi, Effect of different modifier oxides on the synthesis, structural, optical, and gamma/beta shielding properties of bismuth lead borate glasses doped with europium. *J. Mater. Sci. Mater. Electron* (2020). <https://doi.org/10.1007/s10854-020-04662-3>
19. H. Tripathi, C. Rath, A.S. Kumar, P.P. Manna, S.P. Singh, Structural, physicomechanical and in-vitro bioactivity studies on  $\text{SiO}_2-\text{CaO}-\text{P}_2\text{O}_5-\text{SrO}-\text{Al}_2\text{O}_3$  bioactive glasses. *Mater. Sci. Eng.* **94**, 279–290 (2019)
20. N. Elkhoshkhany, R. Abbas, R. El-Mallawany, A.J. Fraih, Optical properties of quaternary  $\text{TeO}_2-\text{ZnO}-\text{Nb}_2\text{O}_5-\text{Gd}_2\text{O}_3$  glasses. *Ceram. Int.* **40**(9), 14477–14481 (2014)
21. H.A. ElBatal et al., In vitro bioactivity behavior of some borophosphate glasses containing dopant of ZnO, CuO or SrO together with their glass-ceramic derivatives and their antimicrobial activity. *Silicon* **11**(1), 197–208 (2019)
22. B. Samanta, D. Dutta, S. Ghosh, Synthesis and different optical properties of  $\text{Gd}_2\text{O}_3$  doped sodium zinc tellurite glasses. *Phys. B Condens. Matter* **515**, 82–88 (2017)
23. D. Maniu, T. Iliescu, I. Ardelean, I. Bratu, C. Dem, *Studies of Borate Vanadate Glasses Using Raman and IR Spectroscopy* (Stud. Univ. Babes-Bolyai Phys, Romania, 2001), pp. 366–371
24. P. Kaur, S. Kaur, G.P. Singh, D.P. Singh,  $\text{Sm}^{3+}$  doped lithium aluminoborate glasses for orange-colored visible laser host material. *Solid State Commun.* **171**, 22–25 (2013)
25. T. Rouxel, Elastic properties of glasses: a multiscale approach. *Comptes Rendus Mec.* **334**(12), 743–753 (2006)
26. D. Saritha, Y. Markandeya, M. Salagram, M. Vithal, A.K. Singh, G. Bhikshamaiah, Effect of  $\text{Bi}_2\text{O}_3$  on physical, optical and structural studies of  $\text{ZnO}-\text{Bi}_2\text{O}_3-\text{B}_2\text{O}_3$  glasses. *J. Non. Cryst. Solids* **354**(52–54), 5573–5579 (2008)
27. G.P. Singh, S. Kaur, P. Kaur, D.P. Singh, Modification in structural and optical properties of ZnO,  $\text{CeO}_2$  doped  $\text{Al}_2\text{O}_3-\text{PbO}-\text{B}_2\text{O}_3$  glasses. *Phys. B* **407**(8), 1250–1255 (2012)
28. M.H.A. Mhareb et al., Impact of  $\text{Nd}^{3+}$  ions on physical and optical properties of lithium magnesium borate glass. *Opt. Mater. (Amst)* **37**, 391–397 (2014)
29. V. Bhatia et al., Mixed transition and rare-earth ion-doped borate glass: structural, optical and thermoluminescence study. *J. Mater. Sci. Mater. Electron.* **30**(1), 677–686 (2019)
30. S. Karki, C.R. Kesavulu, H.J. Kim, J. Kaewkhao, N. Chanthima, Y. Ruangtaweep, Physical, optical and luminescence properties of  $\text{B}_2\text{O}_3-\text{SiO}_2-\text{Y}_2\text{O}_3-\text{CaO}$  glasses with  $\text{Sm}^{3+}$  ions for visible laser applications. *J. Lumin.* **197**, 76–82 (2018)
31. H. Chandler, *Introduction to Hardness Testing* (Hardness testing, USA, 1999), pp. 1–13
32. B. Schrader (ed.), *Infrared and Raman Spectroscopy* (VCH Publ. Inc., New York, 1995), p. 136
33. A.M. Abdelghany, Novel method for early investigation of bioactivity in different borate bio-glasses. *Spectrochim. Acta. Part A.* **100**, 120–126 (2013)
34. S.A. Dalhatu, R. Hussin, K. Deraman, Structural and luminescence properties of  $\text{Eu}^{3+}$ -doped magnesium sulfide borate glass and crystal. *Chinese J. Phys.* **54**(6), 877–882 (2016)
35. M. Karabulut, A. Popa, G. Borodi, R. Stefan, An FTIR and ESR study of iron-doped calcium borophosphate glass-ceramics. *J. Mol. Struct.* **1101**, 170–175 (2015)
36. A.M. Abdelghany, The elusory role of low level doping transition metals in lead silicate glasses. *Silicon* **2**(3), 179–184 (2010)
37. B. Ashok, K.C. Sekhar, B.S. Chary et al., Physical and structural study of  $\text{Al}_2\text{O}_3-\text{NaBr}-\text{B}_2\text{O}_3-\text{CuO}$  glasses. *Indian J Phys* (2021). <https://doi.org/10.1007/s12648-021-02048-7>
38. B.N. Meera, J. Ramakrishna, Raman spectral studies of borate glasses. *J. Non. Cryst. Solids* **159**(1–2), 1–21 (1993)
39. A.A. Osipov, L.M. Osipova, Raman scattering study of barium borate glasses and melts. *J. Phys. Chem. Solids* **74**(7), 971–978 (2013)
40. A.A. Osipov, L.M. Osipova, B. Hruška, A.A. Osipov, M. Liška, FTIR and Raman spectroscopy studies of ZnO-doped  $\text{BaO} \cdot 2\text{B}_2\text{O}_3$  glass matrix. *Vib. Spectrosc.* **103**, 102921 (2019)
41. M.R. Ahmed, B. Ashok, S.K. Ahmmad, A. Hameed, M.N. Chary, M. Shareefuddin, Infrared and Raman spectroscopic studies of  $\text{Mn}^{2+}$  ions doped in strontium aluminoborate glasses: describes the role of  $\text{Al}_2\text{O}_3$ . *Spectrochim. Acta. Part A.* **210**, 308–314 (2019)

42. M.K. Halimah, W.M. Daud, H.A.A. Sidek, A.W. Zaidan, A.S. Zainal, Optical properties of ternary tellurite glasses. *Mater. Sci.* **28**(1), 173–180 (2010)
43. S. Rada, E. Culea, M. Bosca, M. Culea, P. Pascuta, M. Neumann, Effect of the introduction of gadolinium ions in Boro–tellurite glasses. *J. Optoelectron. Adv. Mater.* **10**(9), 2316–2318 (2008)
44. Y.B. Saddeek, Elastic properties of  $Gd^{3+}$ -doped tellurovanadate glasses using pulse-echo technique. *Mater. Chem. Phys.* **91**(1), 146–153 (2005)
45. Y. Al-Hadeethi, M.I. Sayyed, Effect of  $Gd_2O_3$  on the radiation shielding characteristics of  $Sb_2O_3$ – $PbO$ – $B_2O_3$ – $Gd_2O_3$  glass system. *Ceram. Int.* **46**(9), 13768–13773 (2020)

**Publisher's Note** Springer Nature remains neutral with regard to jurisdictional claims in published maps and institutional affiliations.